Transient Capability of the VANGARD GPU-based Pinwise Core Simulator Code

Seoyoon Jeon and Han Gyu Joo*
Seoul National University, 1 Gwanak-ro, Gwanak-gu, Seoul 08826
**Corresponding author: joohan@snu.ac.kr*

1. Introduction

For decades, the conventional two-step core calculation using assembly-homogenized group constants has been adopted as the primary core design method owing to its low computing costs and sufficiently high accuracy required in the industry for the practical applications. However, the need for high-fidelity pin-level solutions has been increased due to stricter safety regulations with reduced margin, which the conventional two-step method cannot provide. Especially for the transient analysis, the use of detailed pin-level solutions is essential in that the assemblywise calculation cannot catch the severe intra-assembly flux gradients occurring near the perturbed rod during a transient [1]. Although a direct whole core calculation code can be used for generating pin-level solutions, it requires too excessive computing resources to be practically employed in the transient analysis which involves repetitive core calculations for more than a thousand time steps. In this regard, a pinwise two-step calculation using pin-homogenized group constants is getting increased attentions as a promising compromise.

In this respect, VANGARD (Versatile Advanced Neutronics code for GPU-Accelerated Reactor Designs) [2], a GPU-based high-speed pinwise nodal core analysis code being developed at Seoul National University, can be a completely suitable core transient analysis tool in that the computing time becomes tolerable even on a PC by exploiting affordable gaming GPUs mounted on it. The simulation capabilities of VANGARD for steady-state and core follow calculations have been verified, and the excellent computing performance has also been confirmed [3]. As a part of the development to make VANGARD a practical pinwise core design code, a transient capability has been developed.

In this work, the transient capability of VANGARD is verified through the analysis of the NEACRP rod ejection benchmark problems [4]. The results of VANGARD are compared with the reference solutions obtained from the direct whole core calculation code nTRACER [5]. In addition, the soundness and the performance of the GPU acceleration for the transient solutions are also evaluated by the comparison between CPU and GPU results on the same code basis.

2. Time-dependent SP3 Formulation

VANGARD employs one-node simplified P3 (SP3) source expansion nodal method (SENM) as the main nodal kernel. In this section, the time-dependent nodal solution of the diffusion and SP3 equations is derived briefly. The detailed derivations including definitions of the temrs can be found elsewhere [6, 7].

The time-dependent multigroup neutron diffusion equation with the precursor balance equation are written as follows:

$$\frac{1}{v_g}\frac{\partial \phi_g}{\partial t} = \chi_g(1-\beta)\psi + \sum_{g'=1}^{G}\Sigma_{g'g}\phi_{g'} + \sum_{k=1}^{6}\chi_{dgk}\lambda_k C_k - \left(\nabla\cdot J_g + \Sigma_{rg}\phi_g\right), \quad (1)$$

$$\frac{dC_k(t)}{dt} = \beta_k\psi(t) - \lambda_k C_k(t). \quad (2)$$

For the temporal discretization, the theta method is applied, which writes Eq. (3) where R_g^n denotes the RHS terms of Eq. (1) at the time step n.

$$\frac{\phi_g^{n+1}-\phi_g^n}{v_g\Delta t_{n+1}} = \theta R_g^{n+1} + (1-\theta)R_g^n \ . \quad (3)$$

In order to obtain the precursor density of the new time step, a quadratic variation of the fission source is assumed, which can be expressed in terms of the known two previous fission sources and the unknown current fission source as follows:

$$C_k^{n+1} = \kappa_k C_k^n + \frac{\beta_k}{\lambda_k}\left(\Omega_k^{n-1}\psi^{n-1} + \Omega_k^n\psi^n + \Omega_k^{n+1}\psi^{n+1}\right). \quad (4)$$

where

$$\Omega_k^{n-1} = \frac{1}{\lambda_k\Delta t_n(\gamma+1)}\left(\frac{2\bar{\kappa}_k}{\lambda_k\Delta t_n} - \gamma(\kappa_k+1)\right),$$

$$\Omega_k^{n} = \frac{1}{\lambda_k\Delta t_n}\left(\kappa_k + 1 + \frac{\bar{\kappa}_k}{\gamma}\left(1-\frac{2}{\lambda_k\Delta t_n}\right)\right) - \kappa_k, \quad (5)$$

$$\Omega_k^{n+1} = 1 - \frac{2}{\lambda_k\Delta t_n(\gamma+1)} + \frac{\bar{\kappa}_k}{\lambda_k\Delta t_n\gamma(\gamma+1)}\left(\frac{2}{\lambda_k\Delta t_n} - 1\right),$$

$$\gamma = \frac{\Delta t_{n+1}}{\Delta t_n},\ \kappa_k = e^{-\lambda_k\Delta t_{n+1}},\ \text{and}\ \bar{\kappa}_k = 1-\kappa_k. \quad (6)$$

By combining Eq. (1), (3), and (4), the transverse-integrated time-dependent neutron diffusion equation for each direction can be represented as follows:

$$-\frac{4D_g}{h^2}\frac{d\phi_g^{n+1}}{d\xi^2}+\Sigma_{rg}\phi_g^{n+1}=\left(\chi_{pg}(1-\beta)+\omega^{n+1}\right)\psi^{n+1}+\sum_{\substack{g'=1\\ g'\neq g}}^{G}\Sigma_{g'g}\phi_{g'}^{n+1} +\frac{\phi_g^n-\phi_g^{n+1}}{\theta v_g\Delta t_{n+1}}+\tilde{s}_{dg}^n-L^{n+1}+\Theta R_g^n, \tag{7}$$

where

$$\tilde{s}_{dg}^n=\sum_{k=1}^{6}\chi_{dgk}\left(\lambda_k\kappa_k C_k^n+\beta_k\left(\Omega_k^{n-1}\psi^{n-1}+\Omega_k^n\psi^n\right)\right),$$
$$\omega_g^{n+1}=\sum_{k=1}^{6}\chi_{dgk}\beta_k\Omega_k^{n+1},\quad \Theta=\frac{1-\bar{\theta}}{\theta}. \tag{8}$$

For the efficient implementations, the equation is rearranged to have the same form with the steady-state equation, and the final form of the time-dependent transverse-integrated neutron diffusion equation is represented as Eq. (9). The only difference from the steady-state solution is that the transient source ($s_{tr,g}^{n+1}$) needs to be additionally calculated. This reformulation enables most of the existing nodal solvers for the steady-state solutions to be directly used for the transient solutions without any modifications.

$$-\frac{4D_g}{h^2}\frac{d^2\phi_g^{n+1}}{dz^2}+\Sigma_{rg}\phi_g^{n+1}=\chi_g\psi^{n+1}+\sum_{g'=1}^{g'=G}\Sigma_{g'g}\phi_{g'}^{n+1}-L_{xy,g}^{n+1}+s_{tr}^{n+1} \tag{9}$$

where

$$s_{tr,g}^{n+1}=s_{fixed,g}^n+\Delta\chi_g\psi^{n+1}-\frac{\phi_g^{n+1}}{\theta v_g\Delta t_{n+1}},$$
$$s_{fixed,g}^n=\tilde{s}_{dg}^n+\frac{\phi_g^n}{\theta v_g\Delta t_{n+1}}+\Theta R_g^n, \tag{10}$$
$$\Delta\chi_g=-\chi_g+\left(\chi_{pg}(1-\beta)+\omega_g^{n+1}\right).$$

Note that the fixed source ($s_{fixed,g}^n$) is determined only by the previous solutions so that it is constant during the current time step. Therefore, it is calculated only once per each time step.

The SP_3 formulation is derived in the analogous manner with the diffusion formulation. The equations are defined for the summed flux and 2nd order moment with differently defined diffusion coefficients and removal cross sections.

$$-\frac{4D_{0,g}}{h^2}\frac{d^2}{d\xi^2}\hat{\phi}_{0,g}+\Sigma_{r0,g}\hat{\phi}_{0,g}=s_{0,g}+s_{tr,0,g},$$
$$-\frac{4D_{2,g}}{h^2}\frac{d^2}{d\xi^2}\phi_{2,g}+\Sigma_{r2,g}\phi_{2,g}=s_{2,g}+s_{tr,2,g} \tag{1}$$

where

$$\hat{\phi}_{0,g}=\phi_{0,g}+2\phi_{2,g},$$
$$D_{0,g}=\frac{1}{3\Sigma_{tr,g}},\ D_{2,g}=\frac{3}{7\Sigma_{t,g}}, \tag{12}$$
$$\Sigma_{r0,g}=\Sigma_{r,g},\ \Sigma_{r2,g}=\frac{4}{3}\Sigma_{r,g}+\frac{5}{3}\Sigma_{t,g}.$$

The source terms are also separately defined. As in the diffusion equation, the total source terms in the SP3 equations are easily obtained by the addition of the transient sources to the steady-state formulations as follows:

$$s_{0,g}=\bar{s}_g+2\Sigma_{r,g}\phi-L_{0,g},\ \ s_{2,g}=-\frac{2}{3}\bar{s}_g+\frac{2}{3}\Sigma_{r,g}\hat{\phi}_{0,g}-L_{2,g},$$
$$s_{tr,0,g}=\tilde{s}_{dg}^n+\Delta\chi_g\psi^{n+1}+\frac{\phi_{0,g}^n-\phi_{0,g}^{n+1}}{\theta v_g\Delta t_{n+1}}+\Theta R_{0,g}^n, \tag{13}$$
$$s_{tr,2,g}=-\frac{2}{3}s_{tr,0,g}+\frac{5}{3}\left(\frac{\phi_{2,g}^n-\phi_{2,g}^{n+1}}{\theta v_g\Delta t_{n+1}}+\Theta R_{2,g}^n\right).$$

In VANGARD, both diffusion and SP3 solutions are implemented and accelerated by GPUs. The SP3 formulation is computationally more expensive than diffusion formulation. Nonetheless, it is superior in terms of accuracy. Therefore, it is more preferable as the main nodal kernel of VANGARD.

3. NEACRP Analysis

For the verification of the transient calculation capability of VANGARD, the 3-dimensional HZP rod ejection problems of NEACRP benchmark [4], namely A1, B1, and C1, were simulated, and the results were compared with those of a direct whole core calculation code nTRACER. The NEACRP benchmark core is composed of 157 fuel assemblies. Each assembly contains 264 fuel rods arranged in 17×17 array, and consists of 18 axial planes including axial reflectors. For all cases, the nominal power of the reactor is 2755 MW, and the ejection time is 0.1 seconds. In the following, the accuracy of the VANGARD transient solutions is provided first and the soundness and performance of the GPU-accelerated transient modules are then confirmed by comparing with the CPU calculation results.

3.1 Verification of transient capability

In both codes, the fully implicit scheme is employed for the time discretization, and the time step sizes are set to 1 ms and 5 ms in VANGARD and nTRACER, respectively. **Figure 1** shows the power distributions of the C1 problem calculated by VANGARD at the steady-state, at the time of core power peak and also at 1.0 second. It clearly shows the significant localized pinwise power increase near the rod-ejected position during the transient, which demonstrates the transient simulation capability of VANGARD. **Table 1** summarizes the calculation results of VANGARD compared with those of nTRACER. **Figure 2** shows the core power behaviors of each problem.

Prior to the analysis of transient results, the steady-state solutions of the diffusion and SP3 calculations were assessed for the ejected rod worth. For the B1 and C1 problems, the rod worths of VANGARD agree with

that of nTRACER within 1 pcm. For the diffusion case of the A1 problem, however, a large overestimation of 29 pcm is noted which leads to a much higher and earlier peak in the transient solution. Even the small difference noted for the SP3 case has a nontrivial impact on core power because the transient core power behavior is strongly dependent on the ejected rod worth [7]. The A1 case demonstrates why the SP3 formulation should be employed in spite of its computational burden.

Meanwhile, for the other cases which do not suffer from the mismatch of the initial condition, all the transient results including the core power and T/H parameters are quite close to the nTRACER results, which verifies the soundness of the transient simulation capability of VANGARD.

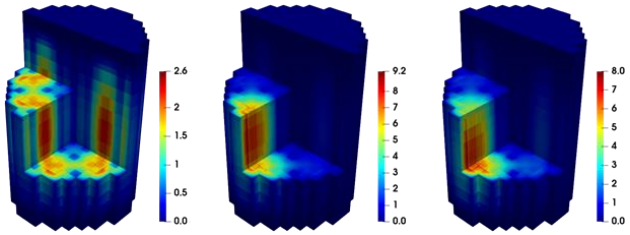

Figure 1. Power distribution of C1 problem at the steady state (left), core power peak (middle), and 1.0 s (right).

Table 1. Comparison between VANGARD and nTRACER results for the NEACRP HZP rod ejection cases.

Parameter	Solver	A1	B1	C1
Ejected Rod worth (pcm)	nTRACER	792.67	824.15	945.97
	Diffusion (Diff.)	821.20 (28.53)	823.17 (-0.98)	944.98 (-0.99)
	SP3 (Diff.)	795.62 (2.95)	824.15 (-)	946.95 (0.98)
Max. Core Power (%)	nTRACER	69.07	236.70	397.42
	Diffusion (Diff.)	137.52 (68.45)	253.25 (16.55)	469.24 (71.82)
	SP3 (Diff.)	78.35 (9.28)	259.38 (22.68)	476.45 (79.03)
Peak Time (s)	nTRACER	0.715	0.515	0.265
	Diffusion (Diff.)	0.538 (-0.177)	0.521 (0.006)	0.267 (0.002)
	SP3 (Diff.)	0.694 (-0.021)	0.516 (0.001)	0.265 (-)
Max. Td* at 5s (℃)	nTRACER	483.12	445.70	519.28
	Diffusion (Diff.)	491.16 (8.04)	452.09 (6.39)	525.14 (5.86)
	SP3 (Diff.)	477.15 (-5.97)	451.57 (5.87)	524.32 (5.04)
Max. Tmod** at 5s (℃)	nTRACER	307.39	302.68	308.19
	Diffusion (Diff.)	309.25 (1.86)	303.12 (0.44)	308.80 (0.61)
	SP3 (Diff.)	307.91 (0.52)	303.04 (0.36)	308.71 (0.52)

* Td: Doppler temperature, ** Tmod: Moderator temperature.

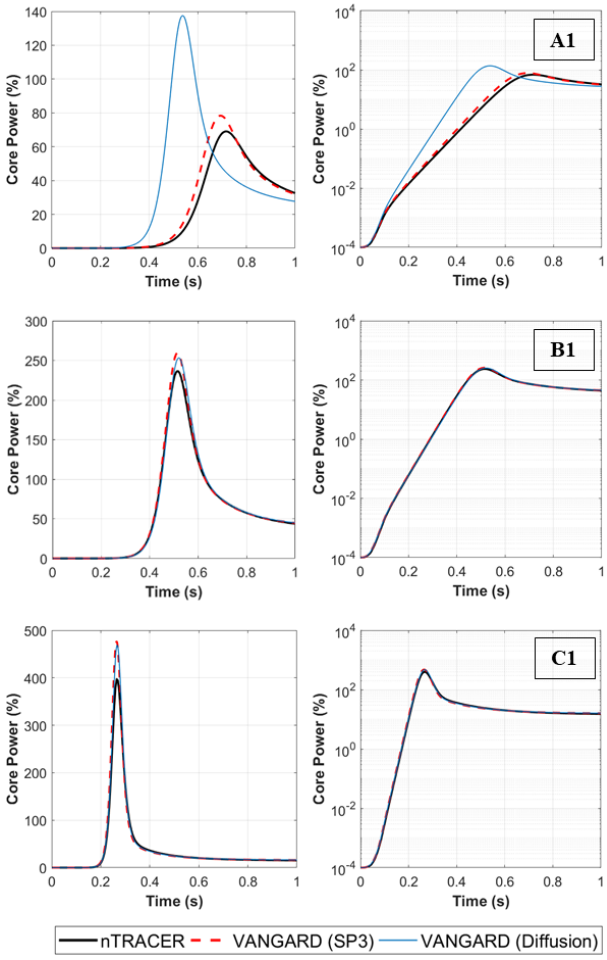

Figure 2. Comparison of core power behaviors.

3.2 Verification of GPU acceleration

Most parts of VANGARD including the nodal solver were programmed such that it can be executed on GPUs as well as on CPUs. The soundness of the GPU-accelerated modules was assessed by the comparison with that of the CPU only case for the C1 problem with the full core geometry. An Intel I9-10900X processor which has 10 cores was used for the CPU calculation parallelized with OpenMP while a single NVIDIA GeForce RTX 3090 was used for the GPU calculation. **Figure 3** shows the core power behaviors from the CPU and GPU calculations and the relative errors between two calculations. The GPU calculation result was confirmed to agree with the CPU calculation result, showing the relative error kept below 0.01%.

Table 2 summarizes the computing times and speedup ratios of the three major GPU-accelerated parts, and **Figure 4** demonstrates the computing time share of CPU and GPU calculations. All the calculations involve 1000 transient steps with time step size of 1 ms. With GPU acceleration, substantial speedups were achieved, especially in the nodal solver which took 95% of the total computing time in the CPU calculation. Owing to

this, the total computing time was reduced from about 9 hours to less than 30 minutes. However, the portion of the T/H calculation which is still performed on CPUs becomes significantly large, taking the largest portion of the total computing time. This issue has not been apparent in the steady-state calculation where it solves the coolant heat transfer equation only once per T/H calculation, owing to the fixed heat source with the concept that all heat generated in the pellet must be delivered to the coolant without accumulation in the fuel. On the contrary, in the transient calculation, the heat source is determined by the fuel temperature profile. It requires coupled iterative solutions, leading to repetitive steam table calculations, which appear to take most parts of the total T/H calculation time. After the completion of the GPU porting of T/H calculation which is under way, the total computing time will be further reduced.

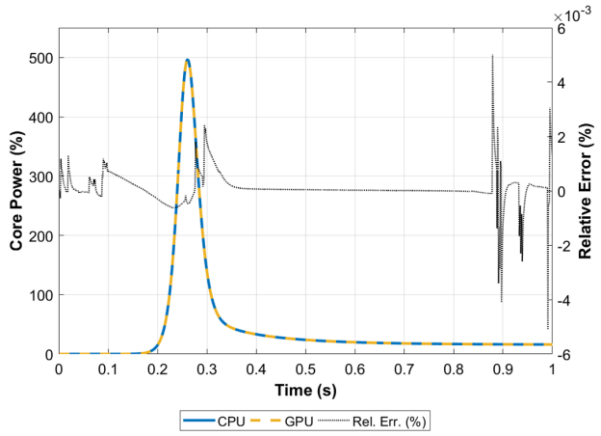

Figure 3. Core power comparison between CPU and GPU calculations.

Table 2. Computing time of the accelerated parts (s).

Calculation	CPU (10 cores)	GPU (single)	Speedup
Nodal	30704.0	637.2	48.2
CMFD	410.5	61.9	6.6
XS	82.2	4.5	18.3
Total	32374.7	1784.1	18.1

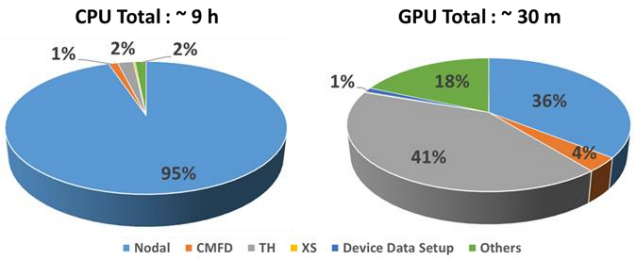

Figure 4. Computing time share comparison.

4. Conclusions

The transient calculation capability of VANGARD was developed and verified with the NEACRP rod ejection benchmark problems. In the comparison with the solution of the MOC-based transport code nTRACER, it was noted that the SP3 solutions match well the higher order solutions. In the case of A1, nontrivial over prediction was noted in the ejected rod with the diffusion solver which leads to a much earlier and higher transient power peak. It confirms that the pinwise SP3 solver is needed in the transient analysis.

The soundness and performance of the GPU acceleration modules were confirmed by the comparison with the CPU calculation results. The core power behaviors were essentially the same. Meanwhile, a single consumer-grade GPU achieved substantial speedups over the 10-core CPU calculation with 48 times speedup in the nodal calculation time and 18 times speedup in the total calculation time. Despite the notable computing time reduction, VANGARD should be further optimized for the practical pinwise core safety analysis. The GPU porting of the T/H feedback calculation which is underway is expected to further improve the performance substantially. In addition, the future work will focus on the performance enhancement by introducing numerical measures needed for using larger time steps with an advanced time marching scheme and for the conditional nodal update.

REFERENCES

[1] A. Facchini, “Development of a Pin Level Thermal/Hydraulics – Neutronics Coupled Core Simulator for High Fidelity Steady-state and Transient Analyses,” Ph.D. Thesis, Seoul National University, Korea (2021).
[2] S. Jeon, H. Hong, N. Choi, H. G. Joo, “GPU Acceleration of the Prototype Pinwise Core Analysis Code VANGARD,” International Conference on Mathematics and Computational Methods Applied to Nuclear Science and Engineering (M&C 2021), Virtual Meeting, Oct. 3-7 (2021).
[3] S. Jeon, H. G. Joo, “Verification and Validation of the GPU-based High-speed Pinwise Nodal Core Analysis Code VANGARD”, Transactions of the Korean Nuclear Society Spring Meeting, Jeju, Korea, May 19-20 (2022).
[4] H. Finnemann, A. Galati, “NEACRP 3-D LWR CORE TRANSIENT BENCHMARK - Final Specifications,” NEACRP-L-335 (Revision 1), OECD Nuclear Energy Agency (1992).
[5] Y. S. Jung, C. B. Shim, C. H. Lim, H. G. Joo, “Practical Numerical Reactor Employing Direct Whole Core Neutron Transport and Subchannel Thermal/Hydraulic Solvers,” Annals of Nuclear Energy 62, pp. 357-374 (2013).
[6] T. Downar, Y. Xu, V. Seker, “PARCS v3.0 U.S. NRC Core Neutronics Simulator Theory Manual,” Department of Nuclear Engineering and Radiological Sciences, University of Michigan, Ann Arbor, MI, September (2009).
[7] C. B. Shim, J. Y. Cho, H. G. Joo, “Application of Source Expansion Nodal Method to SP3 Core Transient Analysis,” Proceedings of the Reactor Physics Asia (RPHA15), Jeju, Korea, Sept. 16-18 (2015).